EXTENDED PDF FORMAT SPONSORED BY Tools for Your **Biological Target**



The Alarmin Interleukin-33 Drives Protective Antiviral CD8⁺ T Cell Responses

Weldy V. Bonilla et al. Science 335, 984 (2012);

DOI: 10.1126/science.1215418

This copy is for your personal, non-commercial use only.

If you wish to distribute this article to others, you can order high-quality copies for your colleagues, clients, or customers by clicking here.

Permission to republish or repurpose articles or portions of articles can be obtained by following the guidelines here.

The following resources related to this article are available online at www.sciencemag.org (this information is current as of June 6, 2012):

Updated information and services, including high-resolution figures, can be found in the online version of this article at:

http://www.sciencemag.org/content/335/6071/984.full.html

Supporting Online Material can be found at:

http://www.sciencemag.org/content/suppl/2012/02/09/science.1215418.DC1.html

A list of selected additional articles on the Science Web sites related to this article can be found at:

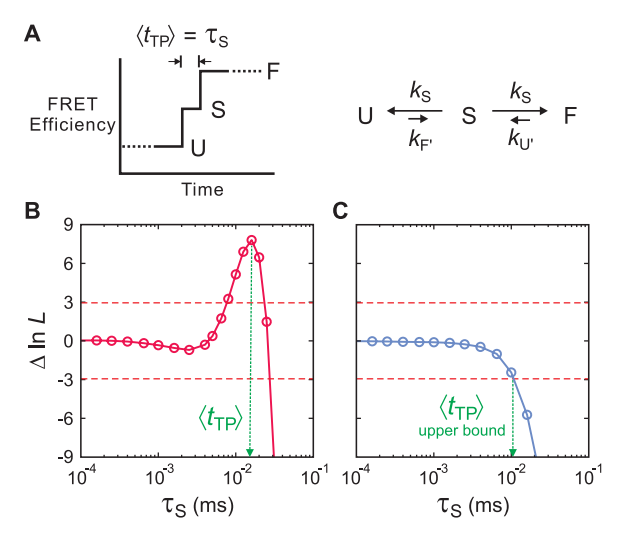
http://www.sciencemag.org/content/335/6071/984.full.html#related

This article **cites 40 articles**, 17 of which can be accessed free: http://www.sciencemag.org/content/335/6071/984.full.html#ref-list-1

This article appears in the following subject collections: **Immunology**

http://www.sciencemag.org/cgi/collection/immunology

Fig. 4. Determination of average transition-path times in a kinetic model. (A) Schematic of a FRET efficiency trajectory using a one-step model to describe the transition path from unfolded (U) to folded (F) states for a protein exhibiting two-state kinetics and thermodynamics. The average transition-path time, $\langle t_{TP} \rangle$, is equal to the lifetime of a virtual intermediate state S $[\tau_S = (2k_S)^{-1}]$. (**B** and **C**) The difference of the log likelihood, $\Delta \ln L = \ln L(\tau_s) - \ln L(0)$, between the two-state model with a finite transitionpath time and a two-state model with an instantaneous transition-path time is plotted as a function of τ_s (B) for the WW domain in 3 M GdmCl in 50% glycerol and (C) for protein GB1 in 4 M urea. The horizontal



dashed line at $\Delta \ln L = +3$ represents the 95% confidence limit for the significance of the peak in (B), and the intersection of the likelihood function with the horizontal dashed line at $\Delta \ln L = -3$ in (C) yields the 95% confidence limit for the upper bound of τ_5 .

is almost the same for two proteins with different topologies and vastly different folding rates.

References and Notes

- J. D. Bryngelson, J. N. Onuchic, N. D. Socci, P. G. Wolynes, Proteins 21, 167 (1995).
- F. Noé, C. Schütte, E. Vanden-Eijnden, L. Reich,
 T. R. Weikl, Proc. Natl. Acad. Sci. U.S.A. 106, 19011 (2009).
- G. R. Bowman, V. S. Pande, Proc. Natl. Acad. Sci. U.S.A. 107, 10890 (2010).
- 4. D. E. Shaw et al., Science 330, 341 (2010).
- S. Piana, K. Lindorff-Larsen, D. E. Shaw, *Biophys. J.* **100**, L47 (2011).
- 6. K. Lindorff-Larsen, S. Piana, R. O. Dror, D. E. Shaw, Science **334**, 517 (2011).

- H. Nguyen, M. Jager, A. Moretto, M. Gruebele, J. W. Kelly, Proc. Natl. Acad. Sci. U.S.A. 100, 3948 (2003).
- M. Petrovich, A. L. Jonsson, N. Ferguson, V. Daggett, A. R. Fersht, J. Mol. Biol. 360, 865 (2006).
- H. S. Chung, J. M. Louis, W. A. Eaton, *Proc. Natl. Acad. Sci. U.S.A.* 106, 11837 (2009).
- 10. I. V. Gopich, A. Szabo, J. Phys. Chem. B 113, 10965 (2009).
- Materials and methods are available as supporting online material on Science Online.
- 12. G. Hummer, J. Chem. Phys. 120, 516 (2004).
- 13. F. Liu, M. Nakaema, M. Gruebele, *J. Chem. Phys.* **131**, 195101 (2009).
- 14. I. C. Yeh, G. Hummer, *J. Phys. Chem. B* **108**, 15873 (2004)
- N. D. Socci, J. N. Onuchic, P. G. Wolynes, J. Chem. Phys. 104, 5860 (1996).

- 16. In the case of protein GB1, there is the possibility of a sparsely populated intermediate between the folded and unfolded states (17–20). In this study, we have implicitly defined the transition-path time for both the WW domain and protein GB1 in terms of just the two deep minima of the folded and unfolded states.
- S. H. Park, M. C. R. Shastry, H. Roder, Nat. Struct. Biol. 6, 943 (1999).
- E. L. McCallister, E. Alm, D. Baker, Nat. Struct. Biol. 7, 669 (2000).
- 19. A. Morrone et al., Biophys. J. 101, 2053 (2011).
- B. A. Krantz, L. Mayne, J. Rumbley, S. W. Englander,
 T. R. Sosnick, J. Mol. Biol. 324, 359 (2002).
- 21. Clarke and co-workers (22) have found, for example, domains with similar structures and stability that have folding rates that differ by ~3000-fold. The slower-folding domains show very little dependence on solvent viscosity, which suggests a large internal friction and, therefore, a much smaller D* (22, 23).
- 22. B. G. Wensley et al., Nature 463, 685 (2010).
- 23. T. Cellmer, E. R. Henry, J. Hofrichter, W. A. Eaton, *Proc. Natl. Acad. Sci. U.S.A.* **105**, 18320 (2008).
- Natt. Acad. Sci. U.S.A. 105, 18320 (2008).
 J. Kubelka, J. Hofrichter, W. A. Eaton, Curr. Opin. Struct. Biol. 14, 76 (2004).
- R. B. Best, G. Hummer, Proc. Natl. Acad. Sci. U.S.A. 102, 6732 (2005).
- J. Kubelka, E. R. Henry, T. Cellmer, J. Hofrichter,
 W. A. Eaton, Proc. Natl. Acad. Sci. U.S.A. 105, 18655 (2008).

Acknowledgments: We thank I. Gopich, A. Szabo, and G. Hummer for numerous helpful discussions and A. Aniana for technical assistance in the expression and purification of proteins. This work was supported by the Intramural Research Program of the National Institute of Diabetes and Digestive and Kidney Diseases, NIH.

Supporting Online Material

www.sciencemag.org/cgi/content/full/335/6071/981/DC1 Materials and Methods Figs. S1 to S9

Table S1

References (27–37)

25 October 2011; accepted 25 January 2012 10.1126/science.1215768

The Alarmin Interleukin-33 Drives Protective Antiviral CD8⁺ T Cell Responses

Weldy V. Bonilla, ^{1,2}* Anja Fröhlich, ^{3,4}* Karin Senn, ⁵* Sandra Kallert, ^{1,2} Marylise Fernandez, ^{1,2} Susan Johnson, ^{1,2} Mario Kreutzfeldt, ^{1,6} Ahmed N. Hegazy, ^{3,4,7} Christina Schrick, ^{1,6} Padraic G. Fallon, ⁸ Roman Klemenz, ⁵ Susumu Nakae, ⁹ Heiko Adler, ¹⁰ Doron Merkler, ^{1,6,11} Max Löhning, ^{3,4}† Daniel D. Pinschewer^{1,2}†

Pathogen-associated molecular patterns decisively influence antiviral immune responses, whereas the contribution of endogenous signals of tissue damage, also known as damage-associated molecular patterns or alarmins, remains ill defined. We show that interleukin-33 (IL-33), an alarmin released from necrotic cells, is necessary for potent CD8⁺ T cell (CTL) responses to replicating, prototypic RNA and DNA viruses in mice. IL-33 signaled through its receptor on activated CTLs, enhanced clonal expansion in a CTL-intrinsic fashion, determined plurifunctional effector cell differentiation, and was necessary for virus control. Moreover, recombinant IL-33 augmented vaccine-induced CTL responses. Radio-resistant cells of the splenic T cell zone produced IL-33, and efficient CTL responses required IL-33 from radio-resistant cells but not from hematopoietic cells. Thus, alarmin release by radio-resistant cells orchestrates protective antiviral CTL responses.

Pathogen-associated molecular patterns (PAMPs) characterize intruding microorganisms and are important for adaptive immune responses to viral infection (1). Conversely, endogenous molecular patterns, which indicate

tissue injury, are referred to as alarmins and form a second class of damage-associated molecular patterns (DAMPs) (2). Unlike PAMPs, the potential contribution of alarmins to antiviral immune defense remains largely elusive. Many viruses are excellent inducers of cytotoxic CD8⁺ T lymphocytes (CTLs) (3), the basis of which is incompletely understood. To screen

¹Department of Pathology and Immunology, University of Geneva, 1 rue Michel Servet, 1211 Geneva 4, Switzerland. ²World Health Organization Collaborating Center for Vaccine Immunology, University of Geneva, Switzerland. 3 Experimental Immunology, Department of Rheumatology and Clinical Immunology, Charité-University Medicine Berlin, Berlin, Germany. ⁴German Rheumatism Research Center (DRFZ), a Leibniz Institute, Charitéplatz 1, 10117 Berlin, Germany. 5 Institute for Cancer Research, Department of Pathology, University Hospital of Zurich, Schmelzbergstrasse 12, 8091 Zurich, Switzerland. ⁶Division of Clinical Pathology, Geneva University Hospital, 1 rue Michel Servet, 1211 Geneva 4, Switzerland. ⁷Department of Gastroenterology, Hepatology and Endocrinology, Campus Charité Mitte, Charité-University Medicine Berlin, Berlin, Germany. ⁸Institute of Molecular Medicine, St. James's Hospital, Trinity College Dublin, Dublin 8, Ireland. 9The Institute of Medical Science, The University of Tokyo, 4-6-1 Shirokanedai, Minato-ku, Tokyo 108-8639, and Japan Science and Technology Agency, Precursory Research for Embryonic Science and Technology (PRESTO), 4-1-8 Hncho, Kawaguchi, Saitama 332-0012, Japan. 10 Helmholtz Zentrum München, Institute of Molecular Immunology and Clinical Cooperation Group Hematopoietic Cell Transplantation (CCG HCT), Marchioninistraße 25, 81377 München, Germany. 11Department of Neuropathology, University Medical Center, Georg August University, Göttingen, Germany.

*These authors contributed equally to this work. †These authors contributed equally to this work. To whom correspondence should be addressed. E-mail: loehning@drfz. de (M.L.); daniel.pinschewer@gmx.ch (D.P.P.) for inflammatory signals augmenting antiviral CTL responses, we used lymphocytic choriomeningitis virus (LCMV) infection of mice. We performed a genome-wide cDNA expression analysis of total spleen tissue from LCMV-infected mice and compared it to an analysis of uninfected controls. From a large panel of interleukins and proinflammatory cytokines, interferon-γ (IFN-γ) and IL-33 were most up-regulated (table S1). The IL-33 receptor ST2, an IL-1 receptor family member also known as T1 and IL1RL1, was also up-regulated.

IL-33 is expressed in the nucleus of nonhematopoietic cells, such as fibroblasts and epithelial and endothelial cells of various tissues (4), but its role in antiviral CTL responses is unknown. Its bioactive pro-inflammatory form is released as a result of necrosis but not apoptosis, classifying IL-33 as an alarmin (5–7). IL-33 mRNA expression peaked at 3 to 5 days after infection and grossly paralleled the kinetics of LCMV RNA (Fig. 1A). To test whether IL-33 was important for CTL responses to LCMV, we performed infection experiments in IL-33–deficient (II33^{-/-}) mice (8). Absence of IL-33 reduced the absolute number of CTLs responding to the immunodominant LCMV epitope GP33 by >90%. The frequency of epitope-specific CTLs was reduced by >75% (Fig. 1B). When expressed as a

nuclear factor in healthy cells, IL-33 is complexed with chromatin and modulates gene expression (9). Upon release from necrotic cells, however, IL-33 binds and signals through ST2 (10, 11). To assess which one of these roles of IL-33 accounted for defective CTL responses in Il33^{-/-} mice, we used transgenic mice expressing a soluble decoy receptor for IL-33 [Il1rl1-Fc mice (12)]. Il1rl1-Fc mice displayed defective CTL expansion analogously to Il33^{-/-} mice (fig. S1A). Mice lacking the IL-33 receptor ST2 [Il1rl1^{-/-} (13)] also mounted similarly reduced responses to all three LCMV epitopes tested (Fig. 1C and fig. S1, B and C). This indicated that

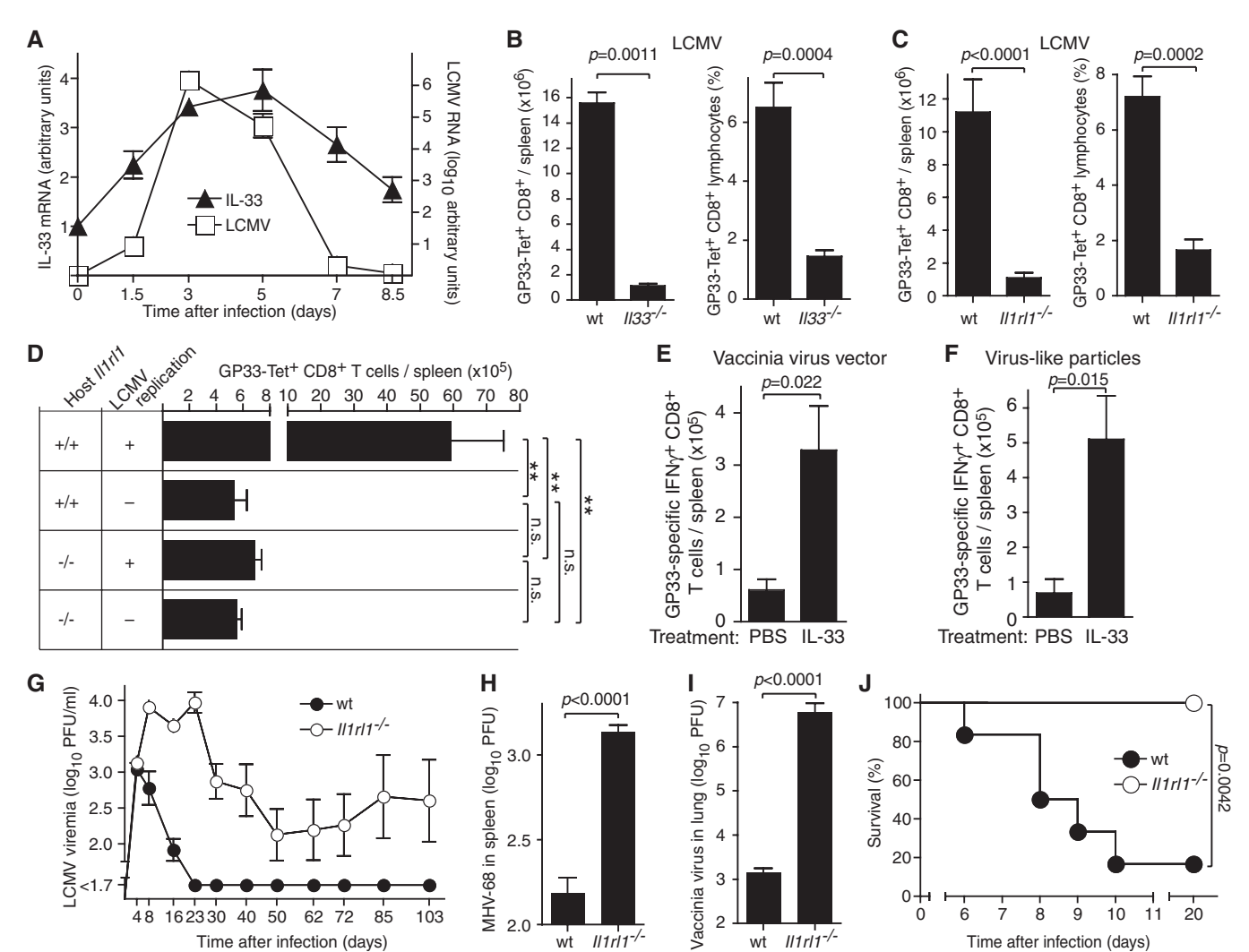


Fig. 1. The IL-33—ST2 pathway drives protective CTL responses to replicating viral infection. (**A**) Kinetic analysis of IL-33 and LCMV RNA expression in the spleen after LCMV infection. Symbols represent the mean \pm SEM of four mice. N=1 (N=1 refers to the number of times an experiment was performed). (**B** and **C**) The number of GP33-specific CTLs in the spleen, as detected by peptide—major histocompatibility complex (MHC) tetramer staining, on day 8 after LCMV infection. Bars represent mean \pm SEM of five mice. N=1 (B) or 3 (C). (**D**) Epitope-specific CTLs of WT and $II1rl1^{-/-}$ mice responding to replicating WT LCMV infection or to replication-deficient rLCMV vectors. Bars represent the mean \pm SEM of five mice. N=2. P<0.0001 by one-way analysis of variance (ANOVA). Results of Bonferroni's posttest are indicated. n.s., not significant; *P<0.05; **P<0.01. (**E** and **F**) WT mice were vaccinated with recombinant VV vector expressing LCMV-GP (E) or with

GP33-carrying VLPs (F) on day 0 and were treated with IL-33 or diluent [phosphate-buffered saline (PBS)] daily from day 1 to 7, and CTL responses were determined on day 8. Bars represent the mean \pm SEM of four to five mice. N=2 (E) or 1 (F). (G) Viremia after infection with 2×10^6 plaqueforming units (PFU) of LCMV-WE. Symbols represent the mean \pm SEM of five mice. N=1. (I) Pulmonary VV titers on day 8 after infection. Bars represent the mean \pm SEM of five mice. N=1. (J) Incidence of choriomeningitis after intracerebral LCMV infection. Terminally diseased animals were killed in accordance with Swiss law. Survival was compared by using the log rank test. Groups of six mice were used. One of two similar experiments is shown. Unpaired two-tailed student's t test was used for statistical analysis in (B), (C), (E), (F), (H), and (I).

IL-33 was released to the extracellular compartment and signaled through ST2 to amplify antiviral CTL responses.

Analogous to the responses against LCMV, an RNA virus, *Il1r11*^{-/-} mice also exhibited significantly reduced CTL responses against murine γ-herpesvirus 68 [MHV-68 (*14*)], a DNA virus (fig. S1D). In further analogy to LCMV, MHV-68 induced IL-33 mRNA up-regulation (fig. S1E). The differences in CTL responses to LCMV and MHV-68 were also reflected in reduced antigenspecific cytotoxicity (fig. S1, F and G). However, CTL responses to a nonreplicating adenovirus-based vaccine vector were similar in *Il1r11*^{-/-} and wild-type (WT) mice (fig. S1H).

Given IL-33 can act as an alarmin, we hypothesized that productive viral replication may represent a unifying characteristic of LCMV and MHV-68 infection, differentiating them from adenoviral vectors. Indeed, the CTL responses of WT and Il1rl1 -- mice to replication-deficient LCMV-based vaccine vector (15) were indistinguishable, and the magnitude of these responses was comparable to the magnitude of responses observed in WT LCMV-infected Il1rl1-/- mice (Fig. 1D). Further, Illrl1^{-/-} mice mounted defective CTL responses against WT vaccinia virus (VV), whereas attenuated [thymidine kinasedeficient (16)] VV-based vectors induced comparable responses in Il1rl1^{-/-} and WT controls (fig. S1I). Thus, we hypothesized that exogenously administered IL-33 could mimic viral replication to enhance vaccine-induced CTL responses. Indeed, recombinant IL-33 significantly augmented CTL responses to VV-based vectors and viruslike particles (VLPs) (Fig. 1, E and F).

CTLs play a pivotal role in the resolution of primary viral infection (14, 17). Il1rl1^{-/-} mice controlled low-dose LCMV infection (fig. S1J) but displayed elevated viremia after high-dose LCMV infection and often progressed to viral persistence, whereas WT control mice eliminated the virus (Fig. 1G and fig. S1K). ST2-deficient mice also displayed a log increase in splenic MHV-68 titers and three logs increase in pulmonary VV titers (Fig. 1, H and I). LCMV-neutralizing antibody responses were comparable in Il1rl1^{-/-} mice and WT controls (fig. S1L), suggesting that defective CTL responses of Il1rl1^{-/-} mice were at the root of impaired LCMV control.

LCMV can cause lethal CTL-mediated immunopathologic disease of the central nervous system when administered intracranially (17). Five out of six WT mice developed terminal disease within 10 days, whereas all Il1rl1^{-/-} mice survived without clinical signs of immunopathology (Fig. 1J).

The IL-33 receptor ST2 has predominantly been detected on mast cells and CD4⁺ T helper type 2 cells (18–20), reportedly exerting pleiotropic effects on helminth-specific immunity, allergy, anaphylaxis, autoimmune, and cardiovascular disease (20, 21). Conversely, ST2 expression on human and mouse CTLs has only recently been found under select in vitro culture and differen-

tiation conditions (22). Hence, we investigated which cells were sensing IL-33 for augmenting antiviral CTL responses. To this end, we reconstituted lethally irradiated mice with an approximately 1:1 mixture of WT (CD45.1⁺) and ST2-deficient bone marrow (CD45.1⁻) (Fig. 2A and fig. S2A).

Compared with uninfected mice, WT cells were 10-fold overrepresented in the population of antigen-specific CTLs responding to LCMV infection (Fig. 2A). In contrast, the repartition of WT and IlIrII^{-/-} B cells remained unaltered (fig. S2A). These observations suggested that virus-reactive

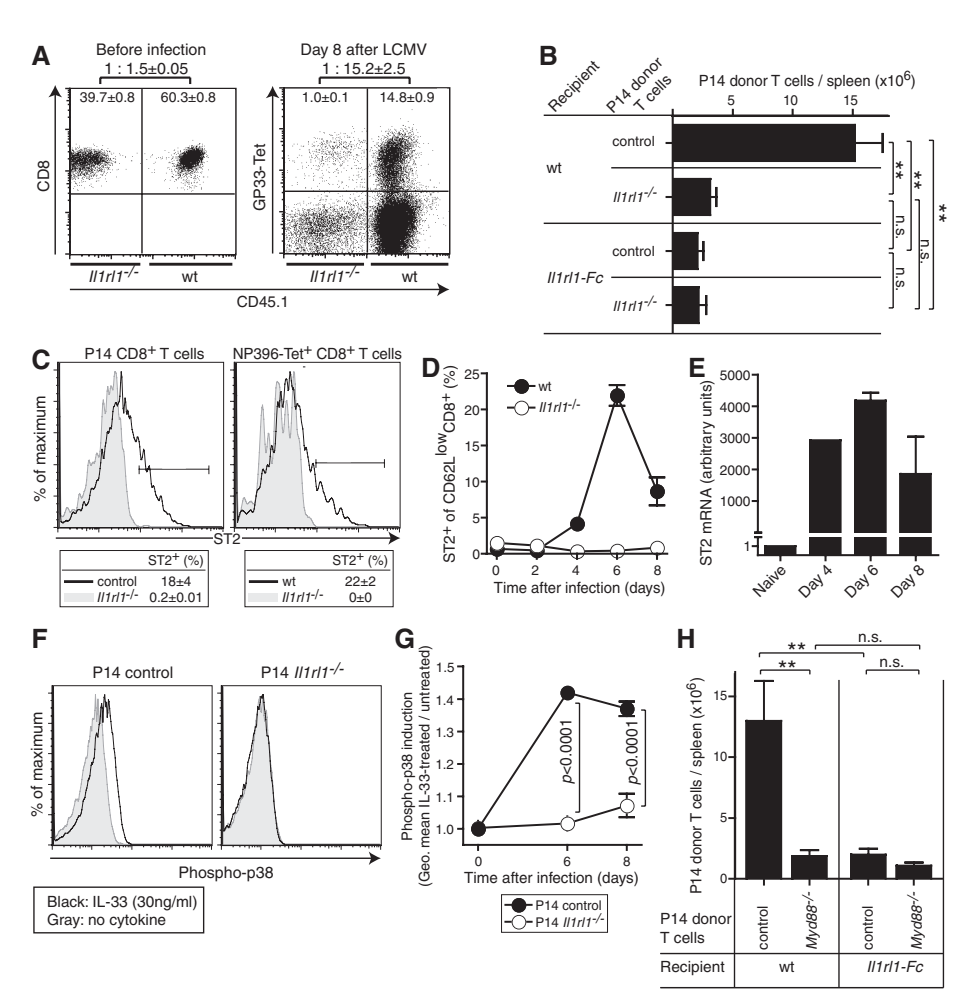


Fig. 2. CD8⁺ T cell—intrinsic signaling through ST2 and MyD88 augments antiviral CTL responses. (A) Irradiated recipients were reconstituted with WT (CD45.1+) and Il1rl1-(CD45.1-) bone marrow. Flow cytometric analysis of WT and Il1rl1--- total CD8+T cells before infection (left) and virus-specific CD8+T cells 8 days after LCMV challenge (right). Values represent mean frequency \pm SEM of three mice. N=2. (B) Control (CD45.1+CD45.2-) and Il1rl1-- (CD45.1+CD45.2+) P14 CD8+ T cells (104) were cotransferred into WT and Il1rl1-Fc recipient mice (CD45.1 CD45.2 and were enumerated on day 8 after LCMV. Bars represent the mean \pm SEM of four mice per group. P < 0.0001 by one-way ANOVA. Results of Bonferroni's posttest are indicated. One representative of three similar experiments is shown. (C) Control and Il1rl1-- P14 cells (104) were individually transferred into WT recipients (left). Peptide-MHC tetramer-binding cells in WT and Il1rl1 - mice were studied (right). On day 6 after LCMV infection, the indicated cell populations in spleen were analyzed for ST2 expression by flow cytometry. Values represent the mean \pm SD of three mice. N=2. (D) Flow cytometric analysis of splenic CD62L^{low}CD8⁺ T cells over time after LCMV infection. Symbols represent the mean \pm SEM of three mice (WT days 2 to 8; $Il1rl1^{-/-}$ day 6) or the mean of two mice (other symbols). N = 2. (E) Quantitative reverse-transcription polymerase chain reaction (qRT-PCR) analysis of ST2 mRNA levels in P14 CD8+ T cells. Day 6 and 8 values represent the mean \pm SEM of three mice. RNA samples from three donor mice were pooled for combined analysis on days 0 and 4. N = 1. (F and G) Flow cytometric analysis of intracellular phospho-p38 expression in control and Il1rl1-- P14 cells isolated on day 6 (F) or over time after LCMV infection and treated ex vivo with recombinant IL-33. Symbols in (G) represent the mean ± SEM of three mice. Unpaired two-tailed student's t test was used for statistical analysis. One representative of two similar experiments is shown. (H) Control (CD45.1+CD45.2-) and Myd88-7-(CD45.1+CD45.2+) P14 cells were cotransferred to WT and Il1rl1-Fc recipient mice (CD45.1-CD45.2+). Expansion was assessed 8 days after LCMV infection. Bars represent the mean \pm SEM of four mice per group. P = 0.0008 by one-way ANOVA. Results of Bonferroni's posttest are indicated. N = 1.

CTLs respond to IL-33 directly. Independent evidence was obtained when T cell receptor-transgenic GP33-specific CTLs (23) (P14 cells) were adoptively transferred, followed by LCMV challenge (Fig. 2B). Impaired expansion of ST2-deficient P14 cells in WT recipients corroborated CTLintrinsic ST2 signaling. As expected, no such differences were seen between control and ST2deficient P14 cells in the IL-33-depleted environment of Il1r11-Fc mice (Fig. 2B). Primary CTL responses to LCMV are CD4 T cell independent (24), and the differences in CTL responses between WT and Illrl1^{-/-} mice persisted when CD4⁺ T cells were depleted (fig. S2B). Altogether, these findings established a CTLintrinsic role of ST2 signaling in the expansion of antiviral CTLs.

On day 6 after LCMV infection, we observed ST2 expression on up to 20% of virus-specific CTLs, representing the peak of expression as monitored on activated (CD62L^{low}) CTLs (Fig. 2, C and D, and fig. S2, C and D). In P14 cells, we detected a simultaneous peak of ST2 mRNA (Fig. 2E). IL-33 signaling through ST2 involves the adaptor protein MyD88 and downstream phosphorylation of p38 mitogen-activated protein kinase (10). Exposure of day 6 LCMV-infected splenocytes to IL-33 ex vivo increased phospho-p38 levels in control P14 cells but not in

ST2-deficient ones (Fig. 2F). In concordance with induction of ST2 expression upon activation, IL-33 failed to trigger detectable phosphop38 signals in naïve P14 cells but did so on day 6 and 8 after infection (Fig. 2G). MyD88 serves important CTL-intrinsic functions, but the upstream receptor(s) accounting for these effects had remained elusive (25). In agreement with previous reports, Myd88^{-/-} P14 cells expanded significantly less than control P14 cells when adoptively transferred into WT recipients and challenged with LCMV (Fig. 2H). In the IL-33depleted environment of Il1rl1-Fc recipients, however, control and Myd88^{-/-} P14 cells responded equivalently, suggesting that defective expansion of Myd88^{-/-} P14 cells was largely attributable to a lack of ST2 downstream signaling.

CTL functionality represents an important correlate of protective capacity (26). A substantial proportion of control P14 effector cells were plurifunctional, co-expressing IFN-γ, tumor necrosis factor (TNF)-α, IL-2, and the degranulation marker CD107a in various combinations (Fig. 3A). Conversely, about 95% of ST2-deficient P14 cells were monofunctional or lacked effector function (Fig. 3A). Reduced plurifunctionality was also observed in polyclonal antiviral CTL populations of ST2-deficient compared with WT mice (fig. S3A). Coexpression of granzyme

B and CD107a indicates efficient cytotoxicity and was nearly undetectable in ST2-deficient P14 cells (Fig. 3B). Control P14 cells also contained significantly higher levels of the anti-apoptotic protein Bcl-2 than ST2-deficient cells (Fig. 3C).

We performed genome-wide cDNA expression profiling of control and ST2-deficient effector P14 cells, yielding 63 differentially expressed candidate genes (fig. S3B and table S2). We validated differential expression of Klrb1c (NK1.1) and Clec2i, which influence effector cell differentiation and proliferation (27, 28); Ifitm1 and *Ifitm3*, which mediate the antiproliferative effects of IFN-y and pro-apoptotic signals (29); and Tspan5, which affects cell proliferation, migration, and adhesion (30); thus corroborating the broad and profound effects of ST2 signals on the CD8⁺ effector T cell transcriptome (Fig. 3D). The gene that encodes KLRG-1, which is a marker of effector CTLs (31), was also among the gene array candidates. Indeed, ST2-deficient P14 cells and virus-specific CTLs of Il1rl1 -- mice exhibited a significant reduction in KLRG-1^{high}CD127^{low} effector CTLs, failed to express NK1.1, and expressed somewhat higher levels of the inhibitory receptor PD-1 (Fig. 3, E and F, and fig. S3, C to E). With transition to the memory phase, however, the size of the LCMV-specific CTL pool and the cells' KLRG-1 expression became similar in WT and

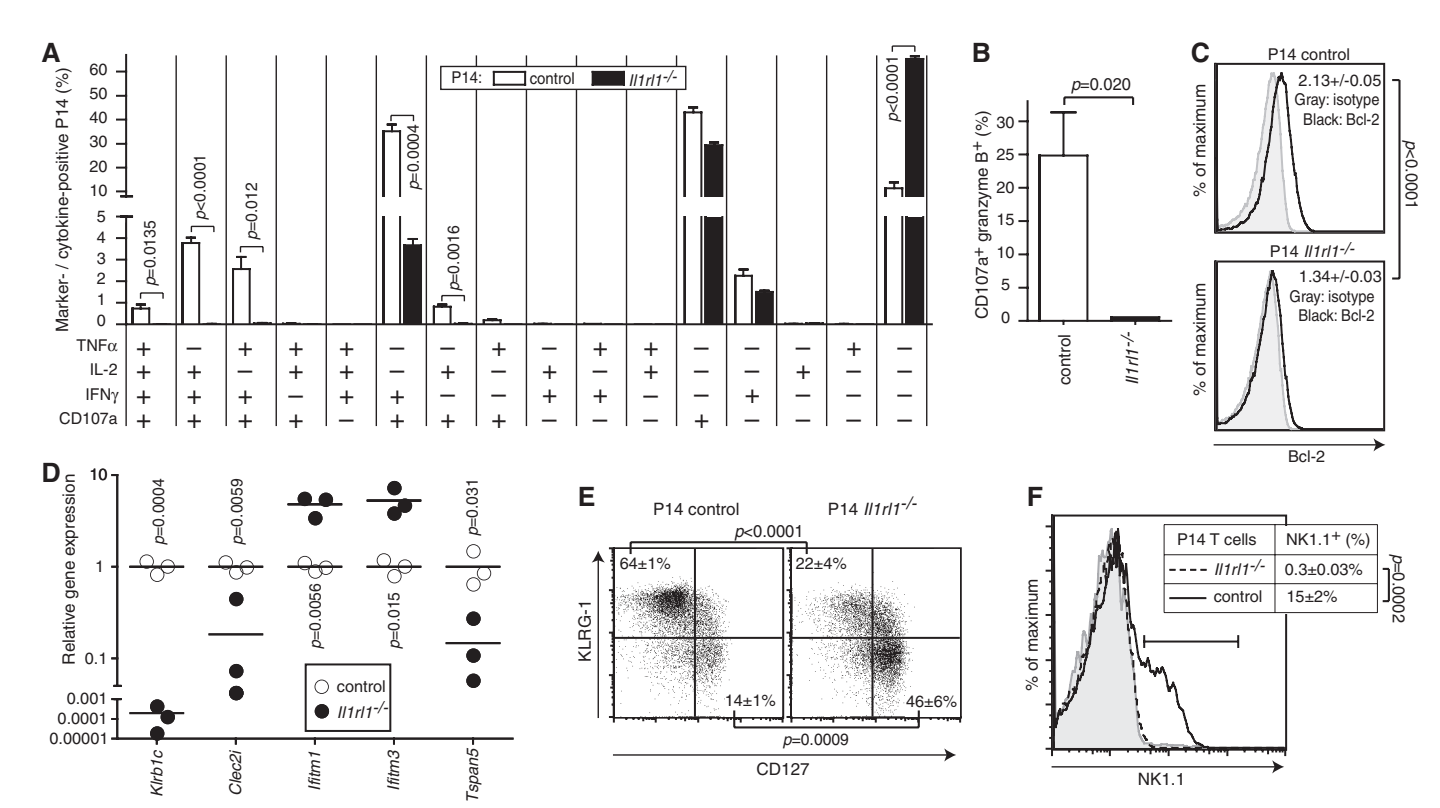
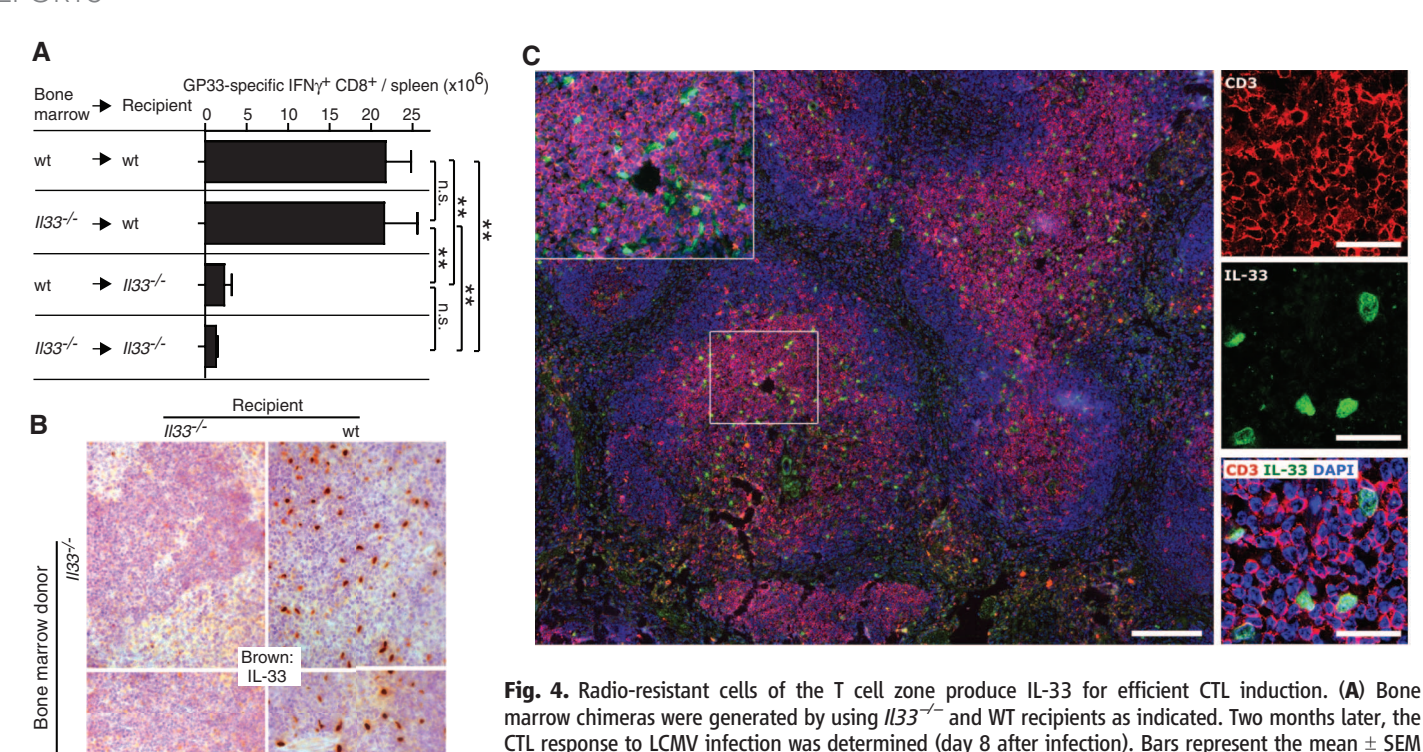


Fig. 3. Broad and profound influence of ST2 signaling on effector CTL differentiation and functionality. (**A** to **C**) CD45.1 $^+$ control and ST2-deficient P14 CD8 $^+$ T cells (10 4) were adoptively transferred into WT recipient mice, which were then challenged with LCMV. Cytokine profile (A), cytolytic phenotype (B), and Bcl-2 expression (C) were assessed on day 8 after LCMV infection. Bars represent mean \pm SEM of three mice. Values in (C) represent geometric mean indices (mean \pm SD of three mice per group). N = 1 [(A) and (B)] or 2 (C). (**D**) Gene

expression profile of P14 cells from recipients as in (A) to (C). The full set of differentially expressed genes is displayed in fig. S3B (also listed in table S2). We validated select genes by qRT-PCR. Symbols show individual mice. N = 1. (**E** and **F**) Phenotypic analysis of splenic $ll1rl1^{-/-}$ and control P14 CD8⁺ T cells from day 8 LCMV-infected WT recipients as in (A) to (C). Values indicate mean \pm SD of three mice. Naïve control P14 T cells are shown as reference in (F) (gray shaded). N = 1. Unpaired two-tailed student's t test was used for statistical analysis.



Spleens from chimeras as in (A) were analyzed for IL-33—expressing cells by immunohistochemistry. The scale bar indicates 50 μm. The image was acquired at 100-fold magnification. Representative pictures from one out of four animals are shown. (C) IL-33+ cells (green) are predominantly found in the T cell zone (characterized by CD3+ T cell clusters, red). DAPI (4′,6′-diamidino-2-phenylindole) was used to stain nuclei (blue). The central white rectangle is displayed at higher magnification in the top left corner of the large image. The small images at right show close vicinity of IL-33+ cells and CD3+ T cells. Scale bars indicate 200 μm (large image) or 50 μm

of five mice. P = 0.0038 by one-way ANOVA. Results of Bonferroni's posttest are indicated. N = 2. (B)

corner of the large image. The small images at right show close vicinity of IL-33" cells and CD3" T cells. Scale bars indicate 200 µm (large image) or 50 µm (small images and inset). Images were acquired at 200-fold magnification by using a slide scanner (large image and inset) and at 400-fold magnification by confocal microscopy (small images). Representative pictures from one out of four mice are shown.

Illrll^{-/-} mice, and vaccinated Illrll^{-/-} mice controlled LCMV challenge infection as efficiently as WT controls (fig. S3, F and G). This supported the concept that inflammatory signals are more important for primary effector CTL responses than for memory formation (25, 32).

To characterize the cellular source of IL-33 bolstering antiviral CTL responses, we generated reciprocal bone marrow chimeras by using WT or Il33^{-/-} mice (Fig. 4A). WT recipient mice generated significantly more LCMV-specific CTLs than Il33^{-/-} recipients, irrespective of the IL-33 competence of the bone marrow. These data suggested that radio-resistant, and thus nonhematopoietic, cells are the main source of IL-33. IL-33⁺ cells were only detected in the spleen of chimeras generated from WT recipients. irrespective of the bone marrow received (WT or 1133^{-/-}, Fig. 4B). IL-33⁺ cells colocalized predominantly with CD3⁺ cells but only sparsely with B cells (Fig. 4C and fig. S4). This was compatible with IL-33 expression by fibroblastic reticular cells (4), a stromal cell population of the T cell zone and known target of LCMV infection (33).

In light of the evidence for IL-33 to act as an alarmin (5, 6), our findings offer a previously unknown molecular link to understand how viral replication, commonly thought of as "danger" (34), can enhance CTL responses to infection.

The nonredundancy with PAMPs is noteworthy, particularly in the context of viral replication, which provides abundant PAMP signals (1). The observed LCMV dose dependency suggests that the IL-33–ST2 axis is most relevant under conditions of high viral burden. We identified nonhematopoietic cells in the splenic T cell zone expressing IL-33. Depending on the site of initiation and expansion of T cell responses, other cell types expressing IL-33 may also supply this cytokine to CTLs (35), and potential regulation by the soluble form of ST2 remains to be investigated (36).

PAMPs act primarily on professional antigenpresenting cells and thereby are decisive for efficient priming of CTLs (37). IL-33 and possibly also other alarmins have complementary and nonredundant functions and, in the case of IL-33, act on antiviral CTLs directly. Taken together, this study establishes a paradigm for the role of nonhematopoietic cells providing alarmins to augment and differentiate protective CTL responses to viral infection.

References and Notes

- 1. D. Schenten, R. Medzhitov, Adv. Immunol. 109, 87 (2011).
- J. J. Oppenheim, D. Yang, Curr. Opin. Immunol. 17, 359 (2005)
- J. W. Yewdell, S. M. Haeryfar, Annu. Rev. Immunol. 23, 651 (2005).

- 4. C. Moussion, N. Ortega, J. P. Girard, *PLoS ONE* **3**, e3331 (2008).
- 5. W. Zhao, Z. Hu, Cell. Mol. Immunol. 7, 260 (2010).
- G. Haraldsen, J. Balogh, J. Pollheimer, J. Sponheim, A. M. Küchler, Trends Immunol. 30, 227 (2009).
- C. Cayrol, J. P. Girard, Proc. Natl. Acad. Sci. U.S.A. 106, 9021 (2009).
- 8. K. Oboki *et al.*, *Proc. Natl. Acad. Sci. U.S.A.* **107**, 18581 (2010).
- V. Carriere et al., Proc. Natl. Acad. Sci. U.S.A. 104, 282 (2007).
- 10. J. Schmitz et al., Immunity 23, 479 (2005).
- 11. C. A. Dinarello, Annu. Rev. Immunol. 27, 519 (2009).
- 12. K. A. Senn et al., Eur. J. Immunol. 30, 1929 (2000).
- M. J. Townsend, P. G. Fallon, D. J. Matthews, H. E. Jolin, A. N. McKenzie, *J. Exp. Med.* 191, 1069 (2000).
- S. Ehtisham, N. P. Sunil-Chandra, A. A. Nash, J. Virol. 67, 5247 (1993).
- 15. L. Flatz et al., Nat. Med. 16, 339 (2010).
- R. M. Buller, G. L. Smith, K. Cremer, A. L. Notkins, B. Moss, *Nature* 317, 813 (1985).
- W. P. Fung-Leung, T. M. Kündig, R. M. Zinkernagel,
 T. W. Mak, J. Exp. Med. 174, 1425 (1991).
- 18. M. Löhning et al., Proc. Natl. Acad. Sci. U.S.A. 95, 6930 (1998).
- 19. D. Xu et al., J. Exp. Med. 187, 787 (1998).
- F. Y. Liew, N. I. Pitman, I. B. McInnes, *Nat. Rev. Immunol.* 10, 103 (2010)
- 21. G. Palmer, C. Gabay, Nat. Rev. Rheumatol. 7, 321 (2011).
- 22. Q. Yang et al., Eur. J. Immunol. 41, 3351 (2011).
- 23. H. Pircher, K. Bürki, R. Lang, H. Hengartner,
- R. M. Zinkernagel, Nature 342, 559 (1989).
- 24. A. Rahemtulla *et al.*, *Nature* **353**, 180 (1991).
- 25. A. H. Rahman et al., J. Immunol. 181, 3804 (2008).
- 26. V. Appay, R. A. van Lier, F. Sallusto, M. Roederer, *Cytometry A* **73**, 975 (2008).
- 27. B. Ljutic et al., J. Immunol. 174, 4789 (2005).

- 28. W. Tian et al., Cell. Immunol. 234, 39 (2005).
- M. J. Dobrzanski, J. B. Reome, J. A. Hollenbaugh,
 R. W. Dutton, J. Immunol. 172, 1380 (2004).
- 30. L. A. Koopman et al., J. Exp. Med. 198, 1201 (2003).
- 31. N. S. Joshi et al., Immunity 27, 281 (2007).
- 32. A. H. Rahman *et al.*, *Blood* **117**, 3123 (2011).
- S. N. Mueller et al., Proc. Natl. Acad. Sci. U.S.A. 104, 15430 (2007).
- S. Gallucci, P. Matzinger, Curr. Opin. Immunol. 13, 114 (2001).
- 35. R. Le Goffic *et al.*, *Am. J. Respir. Cell Mol. Biol.* **45**, 1125 (2011).
- A. Becerra, R. V. Warke, N. de Bosch, A. L. Rothman,
 I. Bosch. Cytokine 41, 114 (2008).
- O. Joffre, M. A. Nolte, R. Spörri, C. Reis e Sousa, Immunol. Rev. 227, 234 (2009).

Acknowledgments: This work was supported by Bundesministerium für Bildung und Forschung (BMBF)—FORSYS (A.F., M.L.), National Health and Medical Research Council (S.J.), German Research Foundation (GRK1121, A.N.H.), Science Foundation Ireland (P.G.F.),

Program for Improvement of Research Environment for Young Researchers, the Special Coordination Funds for Promoting Science and Technology from the Japanese Ministry of Education, Culture, Sports, Science and Technology, Japan Science and Technology Agency, PRESTO (S.N.), BMBF (NGFNplus, FKZ PIM-01GS0802-3; H.A.), Wilhelm Sander-Stiftung (H.A.), German Research Foundation (SFB618 and SFB650, M.L.). Volkswagen Foundation (Lichtenberg Program, M.L.), Fondation Leenaards (D.D.P.), European Community (D.D.P.), and Swiss National Science Foundation (D.M., D.D.P.). We thank A. Bergthaler, G. R. Burmester, C. Gabay, M. Geuking, A. Kamath, P. H. Lambert, J. Luban, B. Marsland, G. Palmer, A. Radbruch, C. A. Siegrist, and R. M. Zinkernagel for discussions and advice; H. Saito, National Research Institute for Child Health and Development, for Il33^{-/-} mice obtained under a materials transfer agreement (MTA) through the RIKEN Center for Developmental Biology, Laboratory for Animal Resources and Genetic Engineering; A. McKenzie (for Il1rl1-/mice obtained under MTA); the University of Zurich (for rLCMV technology obtained under MTA) and G. Jennings [Cytos Biotechnology AG, Schlieren, Switzerland, holding patent rights on VLPs provided] for reagents; and J. Weber and B. Steer

for technical assistance. The data presented in this paper are tabulated in the main paper and the supporting online material. Microarray data are deposited with National Center for Biotechnology Information Gene Expression Omnibus (GEO, accession number GSE34392) and ArrayExpress (accession number E-MTAB-901). D.D.P. is or has been a shareholder, board member, and consultant to ArenaVax AG, Switzerland, and to Hookipa Biotech GmbH, Austria, commercializing rLCMV vectors (patent application EP 07 025 099.8, coauthored by D.D.P.). The authors declare that they do not have other competing financial interests.

Supporting Online Material

www.sciencemag.org/cgi/content/full/science.1215418/DC1 Materials and Methods Figs. S1 to S4 Tables S1 and S2 References (38–40)

18 October 2011; accepted 20 January 2012 Published online 9 February 2012; 10.1126/science.1215418

The Cellular Basis of GABA_B-Mediated Interhemispheric Inhibition

Lucy M. Palmer, ¹ Jan M. Schulz, ¹ Sean C. Murphy, ¹ Debora Ledergerber, ¹ Masanori Murayama, ² Matthew E. Larkum^{1,3}*

Interhemispheric inhibition is thought to mediate cortical rivalry between the two hemispheres through callosal input. The long-lasting form of this inhibition is believed to operate via γ -aminobutyric acid type B (GABAB) receptors, but the process is poorly understood at the cellular level. We found that the firing of layer 5 pyramidal neurons in rat somatosensory cortex due to contralateral sensory stimulation was inhibited for hundreds of milliseconds when paired with ipsilateral stimulation. The inhibition acted directly on apical dendrites via layer 1 interneurons but was silent in the absence of pyramidal cell firing, relying on metabotropic inhibition of active dendritic currents recruited during neuronal activity. The results not only reveal the microcircuitry underlying interhemispheric inhibition but also demonstrate the importance of active dendritic properties for cortical output.

The connection between the two hemispheres of the cerebral cortex via the corpus callosum is one of the most studied and yet least understood pathways in the brain (1, 2). An important function of transcallosal fibers is to mediate interhemispheric inhibition (3, 4), which influences fine motor control (5, 6), visuospatial attention (7-9), and somatosensory processing (10, 11). To investigate the cellular mechanisms of interhemispheric inhibition, we performed in vivo patch-clamp recordings from layer 5 (L5) pyramidal neurons in the hindlimb area of the somatosensory cortex in urethane-anesthetized rats (Fig. 1A). Stimulation of the contralateral hindpaw (contralateral HS) (1-ms duration, 100 V) increased the baseline firing rate by a factor of about 3 (0.9 \pm 0.2 to 2.9 \pm 0.6 Hz; P < 0.05; n = 19)

¹Physiologisches Institut, Universität Bern, Bühlplatz 5, CH-3012 Bern, Switzerland. ²Behavioral Neurophysiology Laboratory, Brain Science Institute, Riken, 2-1 Hirosawa, Wako, Saitama 351-0198, Japan. ³Neurocure Cluster of Excellence, Department of Biology, Humboldt University, Charitéplatz 1, 10117, Berlin, Germany.

*To whom correspondence should be addressed. E-mail: matthew.larkum@gmail.com

(Fig. 1, B to D, black). Ipsilateral hindpaw stimulation (ipsilateral HS), on the other hand, had little influence on the firing rate (1-ms duration, 100V; spontaneous, 1.1 ± 0.2 Hz and evoked, 1.2 ± 0.2 Hz; n = 19 (Fig. 1B, green). However, an inhibitory influence of ipsilateral HS could be uncovered by pairing it with contralateral HS (paired HS). Here, paired HS resulted in a significant decrease in evoked firing (evoked, 2.2 ± 0.5 Hz; n = 19; P < 0.05) when the ipsilateral hindpaw was stimulated 400 ms before the contralateral hindpaw (Fig. 1, B to D, blue). This influence of paired HS on action potential (AP) generation occurred throughout the entire evoked excitatory response, which lasted on average $513 \pm 49 \text{ ms } (n = 19) \text{ (Fig. 1C, gray area)}. \text{ Un-}$ expectedly, paired HS had no discernible effect on the subthreshold responses (Fig. 1, B to D), which did not significantly decrease in average area $(3.4 \pm 0.6 \text{ versus } 3.4 \pm 0.6 \text{ mV} \cdot \text{s}; n = 20) \text{ nor}$ variance (15.7 \pm 1.9 versus 17.2 \pm 02.1 mV²; n =20) (fig. S1).

The average 25 ± 8% decrease in the evoked firing during paired HS was somatotopically specific because stimulation of different regions

of the body, or even different parts of the hindlimb, did not reduce the response to contralateral HS (fig. S2). Furthermore, the decrease in firing did not occur when the contralateral hindpaw was stimulated twice at an interval of 400 ms (fig. S3), and paired HS had no inhibitory effect on layer 2/3 (L2/3) pyramidal neurons (contralateral HS, 3.9 ± 0.6 Hz; paired HS, 3.6 ± 0.7 Hz; t = 400ms; n = 9) (fig. S4). When the timing of the paired-HS interval was varied in 200-ms steps, L5 pyramidal neuron firing was only influenced when the ipsilateral hindpaw was stimulated either 200 or 400 ms before the contralateral hindpaw (Fig. 1E). The long-time course for this type of inhibition suggested the involvement of γ-aminobutyric acid type B (GABA_B) receptors, which can exert an effect for up to 500 ms in vitro (12). Indeed, application of the GABA_B-receptor antagonist, CGP52432 (1 µM) to the cortical surface blocked the decrease in firing generated by paired HS (contralateral HS, 1.9 ± 0.7 Hz; paired HS, 2.0 ± 0.9 Hz, t = 400 ms; n = 8) (Fig. 1E).

It has been suggested in humans that ipsilateral somatosensory stimulation leads to suppression of sensory responses due to transcallosal inhibition (13). We tested this hypothesis in rats using optogenetic stimulation of the transcallosal pathway in vivo. Deep-layer neurons infected with channelrhodopsin-2 (ChR2) conjugated with adenovirus (AAV) sent callosal fibers predominantly to the upper layers of the opposite hemisphere (Fig. 2A and fig. S5) [see supporting online material (SOM)]. Photostimulation (470 nm; trains of 10- by 10-ms pulses at 10 Hz, beginning 400 ms before the sensory stimulus) of callosal input decreased the evoked firing rate of L5 pyramidal neurons by $36 \pm 15\%$ when the light was focused above the hemisphere containing the recording electrode (n = 9; P < 0.05) (Fig. 2, B and C) and by $38\% \pm 14\%$ with photostimulation of the injected hemisphere (n = 7; P < 0.05) (fig. S6). Photoactivation of the callosal fibers alone did not influence spontaneous firing activity $(0.6 \pm 0.2 \text{ Hz prephotoactivation and } 0.7 \pm 0.3 \text{ Hz})$ during photoactivation) (fig. S6), and there was